Research & Reviews: Journal of Material Sciences e-ISSN: 2321-6212

Synthesis of MnO_2 with Different Morphologies and Characterization by Oxygen Isotope Exchange Technology

Dasong Peng, Xiaodong Wang*, Yanchao Ren, Ziyue Tan, Shanping Hu

Quanzhou Yunjian Measurement Control and Perception Technology Innovation Research Institute, Fujian Province, China

Research Article

Received: 15-Mar-2022, Manuscript No. JOMS-22-54482; **Editor assigned:** 17- Mar-2022, PreQC No. JOMS -22-54482(PQ); **Reviewed:** 29- Mar -2022, QC No. JOMS -22-54482; **Revised:** 31- Mar -2022, Manuscript No. JOMS -22-54482(R); **Published:** 07- Apr-2022, DOI: 10.4172/2321-6212.10.3.001.

***For Correspondence:**

Xiaodong Wang, Quanzhou Yunjian Measurement Control and Perception Technology Innovation Research Institute

E-mail:

wangxiaodong8530@126.com

Keywords: MnO_2; Diverse morphologies; CO oxidation; Oxygen isotopic exchange technology

ABSTRACT

As a typical spinel-structure transition metal, manganese dioxide has attracted considerable attention. In this study, by hydrothermal and calcinating methods, the MnO_2 samples of Nanoflower (NF), Nanococoon (NC), Nanotube (NT) and Nanoslice (NS) have been synthesized. Physicochemical properties of these materials are characterized by XRD, N_2 sorption, SEM, XPS, H_2-TPR. And by Oxygen Isotopic Exchange (OIE) technology, their transfer ability for oxygen is evaluated for the first time. The results show that NF sample (Surface area=97.3m^2/g) possesses much higher adsorbed oxygen and much better low-temperature reducibility than other samples. In the $^{18}O_2$ exchange reaction, the NF sample shows the best transfer ability for surface and bulk oxygen. It is concluded that the excellent catalytic performance towards CO over NF-MnO_2 sample is associated with abundant specific surface area, surface oxygen species concentration, good low temperature reducibility and better transfer ability for oxygen.

INTRODUCTION

The physicochemical properties of materials have great relationship with the compositions, intrinsic crystal structures, morphologies and microstructures. Thus, great attention has been given to design various micro/nanostructures. For the possible substitutes for noble metals and excellent properties in this area of catalysis and lithium-ion batteries, the research of synthetizing different morphology micro/nano-MnO_2 has attracted extensive study. Many articles have been devoted to the synthesis, characterization and reactivity of MnO_2 [1-4]. The research in this field has made great achievements. According to the literature, the synthesis of MnO_2 with different morphologies has been widely investigated using a variety of techniques. As catalyst, MnO_2 has used in many fields, such as the elimination of CO [1-5], methanol [6], alcohol [7], formaldehyde [8], toluene [9]. To design various micro/nanostructures, find the possible substitute of noble metal and get excellent properties of catalysts

and lithium-ion battery, series of works have been done on the research of synthesizing micro/nano-MnO_2 with different morphologies [9-11] and great achievements have been obtained.

The study of this work is focused on the combustion of CO. In this work, four different morphologies of MnO_2 have been obtained. Traditional characterizations were carried out by means of various techniques such as XRD, N_2 sorption, SEM, XPS, and H_2-TPR. Moreover, a comparative investigation was carried out to study the oxygen transfer behaviour by using Oxygen Isotopic Exchange (OIE) technology, which is beneficial for providing an insight into the related oxidation mechanism occurring over these materials and elucidating the role of surface and bulk oxygen.

MATERIALS AND METHODS

Neodymium-the catalyst preparation

In this work, four different morphologies of MnO_2 have been obtained by hydrothermal and calcinating methods, namely Nanoflower (NF), Nanococoon (NC), Nanotube (NT), and Nanoslice (NS).

Synthesis of NF sample: The steps we used to synthesize the NF sample were as follows:

Step 1: Mixed 0.676 g $MnSO_4 \cdot H_2O$ with 0.948 g $KMnO_4$, and let stand for 30 minutes.

Step 2: Added 40 ml deionized water into the mixture.

Step 3: Placed the solution into a Teflon-lined stainless steel autoclave whose capacity was 100 ml.

Step 3: Sealed the autoclave and hydrothermally treated the sample solution in autoclave at 50℃ for 4 h, then, cooled it down to room temperature naturally.

Step 4: Collected the precipitate by filtration and washed it several times using deionized water.

Step 5: Dried the sample at 80℃ for 24 h.

Synthesis of NC sample: The steps we used to synthesize the NC sample are as follows:

Step 1: Add 6.7 g $MnSO_4 \cdot H_2O$ into 50 ml deionized water.

Step 2: Add 5.3 ml HNO_3 into the last step's solution with stirring.

Step 3: Place the solution into a Teflon-lined stainless steel autoclave whose capacity is 100 ml.

Step 4: Seal the autoclave and hydrothermally treat at 120℃ for 24 h, then, cool it down to room temperature naturally.

Step 5: Collect the precipitate by filtration and wash it several times using deionized water.

Step 6: Dry the sample at 80℃ for 24 h.

Synthesis of NT sample: The steps we used to synthesize the NT sample are as follows:

Step 1: Add 6.7 g $MnSO_4 \cdot H_2O$ into 50 ml deionized water.

Step 2: Add 4.2 ml HNO_3 into the solution with stirring.

Step 3: Place the solution into a Teflon-lined stainless steel autoclave whose capacity is 100 ml.

Step 4: Seal the autoclave and hydrothermally treat at 120℃ for 12 h, then, cool it down to room temperature naturally.

Step 5: Collect the precipitate by filtration and wash it several times using deionized water.

Step 6: Dry the sample at 80℃ for 24 h.

Synthesis of NS sample: The steps we used to synthesize the NS sample are as follows:

Step 1: Add 5 g $KMnO_4$ into 50 ml deionized water.

Step 2: Place the solution into a Teflon-lined stainless steel autoclave whose capacity was 100 ml.

Step 3: Seal the autoclave and calcined with a ramp of 10℃/min to 120℃, then, cool it down to room temperature naturally.

Step 4: Collect the precipitate by filtration and wash it several times using deionized water.

Step 5: Dry the sample at 80℃ for 24 h.

Characterization

These as-prepared samples were characterized by several techniques including XRD, N_2-sorption, SEM, XPS, and H_2-TPR.

Isotopic Oxygen Exchange (OIE) reaction

Oxygen isotopic exchange and equilibration methods were generally used to evaluate oxygen mobility [12]. The exchange reaction mechanism can be described by the following Equation (1):

$$^{18}O\ (g)+^{16}O\ (s) \leftrightarrow {}^{18}O\ (s)+^{16}O\ (g) \quad (1)$$

Where (s) and (g) refer to the solid and the gas phase, respectively. Nevertheless, three mechanisms can be distinguished depending on the different kinds of oxides: equilibration reaction, simple heteroexchange, and complex heteroexchange. The equilibration reaction mechanism is due to the adsorption/desorption of an O_2 molecule from the gas phase on the surface of oxide. This process does not require the participation of any oxygen ion from the oxide. Then, the ^{18}O and ^{16}O fractions in the gas phase are constant during the test. This reaction can be described by the following Equation (2):

$$^{18}02\ (g)+^{16}02\ (g) \leftrightarrow 2^{18}O^{16}O\ (g) \quad (2)$$

The equilibration reaction mechanism does not involve the participation of oxygen from the solid, so it is normally used to evaluate the material surface reactivity at low temperature. While simple and complex heteroexchange mechanisms occur with the participation of oxygen ion from the structure of the solid. It is considered as simple heteroexchange when one oxygen atom is involved to exchange process, which is applied to most of simple oxides.

However, two atoms of oxygen from the solid exchanging in one step suggest it is attributed to complex heteroexchange, which occurs to some oxides such as CuO, AgO and CeO_2 [12]. The simple heteroexchange and complex heteroexchange processes can be described by the following Equations (3) and (4), respectively.

$$^{18}O^{18}O\ (g)+^{16}O\ (s) \leftrightarrow {}^{16}O^{18}O\ (g)+^{18}O\ (s) \quad (3)$$

$$^{18}O^{18}O\ (g)+ 2^{16}O\ (s) \leftrightarrow {}^{16}O^{16}O\ (g)+2^{18}O\ (s) \quad (4)$$

Therefore, bulk oxygen mobility of catalyst is determined by using simple heteroexchange or complex heteroexchange reactions at high temperature for the participation of solid oxygen.

Catalytic performance measurement

CO oxidation reactions were performed in a tubular microreactor. 200 mg of material was inserted inside the reactor. All the samples pretreatments were performed at 100°C temperatures for 1 h in a stream of air in order to remove the previous absorbates from the as-prepared samples surface, and then cooled down to 0˚C for CO oxidation. The reaction gas mixtures composed of 2 vol% of CO, 20 vol.% of O_2, and balanced by Ar with a total flow rate of 100 ml/min were further fed into the catalyst bed.

RESULTS AND DISCUSSION

XRD pattern of the catalysts

The Samples were analyzed by X-ray diffractometer (D8, Siemens), Cu-Kα ray, 40 kV, 40 mA, 2θ range of 10°-80°, scanning speed 4°C/min. Figure 1 presents the XRD patterns of the as-prepared MnO_2 samples. For the NF sample, the weak diffraction peaks indicate that the crystallinity is low, and the XRD pattern is difficult to match a certain crystal form because of the weak diffraction peaks [8]. Refer to other literatures, the NC and NT samples are identified to pure α-MnO_2 (JCPDS No.44−0141) [13,14]. For the NS sample, the sample is identified to δ-MnO_2 (JCPDS 80-1098) [15,16].

Figure 1. XRD patterns of MnO_2 samples prepared through different methods (a: NF, b: NC, c: NT, d: NS).

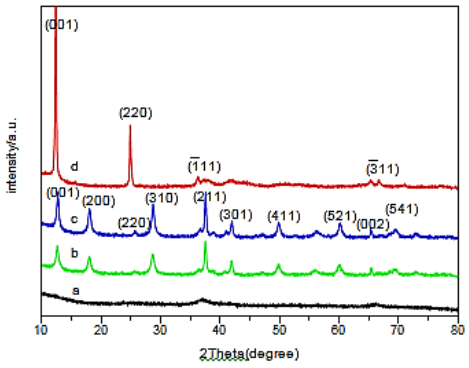

Morphology and surface area

The MnO_2 samples were analyzed by scanning electron microscopy, and the used equipment was JSM-6510A (JEOL). Figure 2 shows the SEM images of the four catalyst samples. From the images, we can see that the morphologies of four samples have great difference under magnification.

Figure 2. SEM of MnO_2 samples: (A) NF, (B) NC, (C) NT, (D) NS.

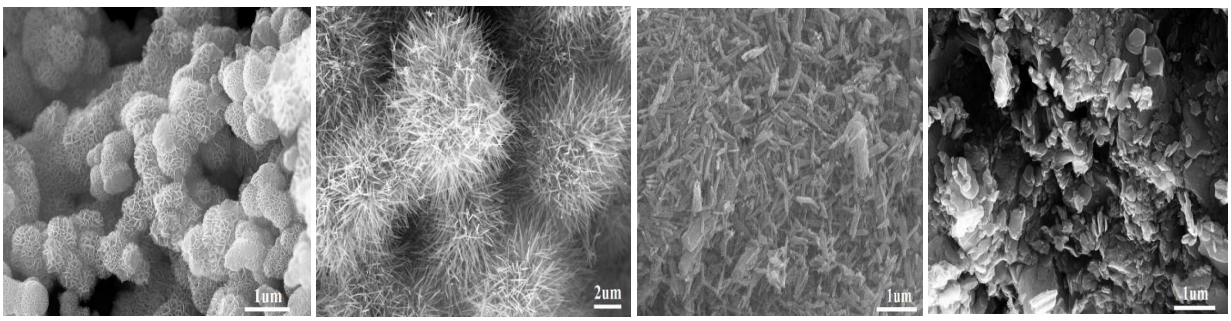

A. B. C. D.

Table 1. The BET of MnO_2 samples.

Samples	BET surface area (m^2/g)
NF	97.3
NC	41.5
NT	29.8
NS	18.2

The specific surface area of the sample was determined on the static nitrogen adsorption instrument (JW-RB24). Before determination, the samples should be pretreated at 200°C for 3 h. The specific surface areas of these MnO_2 catalyst samples are shown in Table 1. It can be observed that the specific surface area (97.3 m^2/g) of the NF sample is much larger than the other samples. The differences of specific surface area are obvious.

X-Ray Photoelectron Spectroscopy (XPS)

The element content and valence state on the sample surface were detected and analyzed by X-Ray Photoelectron Spectroscopy (XPS). The used equipment was ESCALAB 250 (Thermo-Fisher Company). The different valence states of the same element are quantitatively analyzed by peak fitting of the spectrum of related elements, and the fitting follows the quantum rules. XPS of as-prepared MnO_2 catalyst samples were employed to analyse the elemental composition of surface and subsurface layers, and clarify the characteristic of active sites. The XPS results are shown in Figure 3, in which the Mn $2p^{3/2}$ and Mn $2p^{1/2}$ respectively peaked at 642.3 and 654 eV, which can be attributed to Mn^{4+}[1,15,17]. This means that the manganese species mainly exist in a MnO_2 form. This result is consistent with that of XRD, and there is no other valence manganese.

Figure 3. Mn 2p XPS spectras: a (NF), b (NC), c (NT), d (NS).

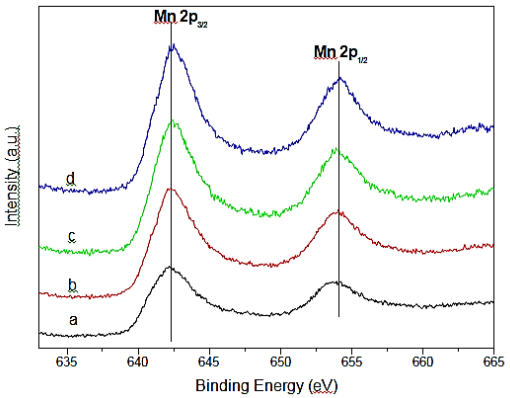

Figure 4. (A) O1 s and (B) O1 s XPS spectras: a (NF), b (NC), c (NT), and d (NS).

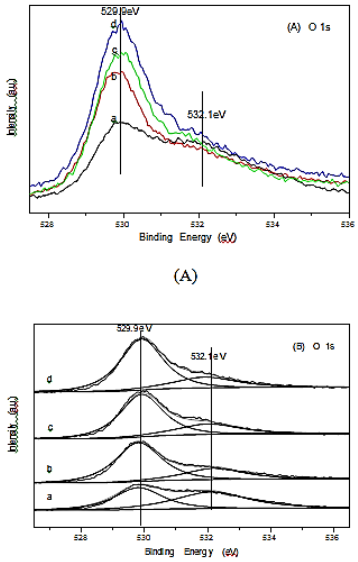

For the O1s XPS spectrogram (shown in Figure 4), two asymmetric peaks can also be obtained for each sample, and two components at binding energy (BE=529.9 and 532.1 eV) can be decomposed [1,15,17]. It can be attributed to the surface lattice oxygen (O_{latt}) species for the former and the surface adsorbed oxygen (O_{ads}) species for the latter. The quantitative results (Table 2) reveal that the O_{ads}/O_{latt} molar ratio (1.15) of NF is markedly higher than the others. The NC and NT samples show similar O_{ads}/O_{latt} molar ratio. For NS, the O_{ads}/O_{latt} molar ratio is only 0.29, which indicates that the sample has less oxygen ad-species than the NF sample. According to the literature [18], more oxygen ad-species can promote the facile activation of O_2 molecules on the manganese oxide. According to the present results and literature [19], the CO combustion follows surface oxidation reduction mechanism, and the oxygen which participated in reaction is mainly the surface oxygen for the CO combustion temperature is low. For NS sample, the high efficiency of CO combustion is caused by the good ability of adsorption and activation of O_2 molecules, and the large molar ratio of O_{ads}/O_{latt}.

Table 2. Surface element compositions of the MnO_2 samples.

Samples	Surface element composition O_{ads}/O_{latt}
NF	1.15
NC	0.37
NT	0.35
NS	0.29

Temperature Programmed Reduction (TPR)

Temperature Programmed Reduction (H_2-TPR) experiments were used to evaluate the redox abilities of solid catalysts. The experiments were carried out on a fixed bed micro reactor. Accurately weigh 100 mg of catalyst and raise it from 100°C to 800°C at the heating rate of 10°C /min under the mixed gas flow of 5% H_2/Ar (40 ml/min, STP). After the tail gas was cooled and dewatered, the hydrogen consumption was detected by Gas Chromatography (GC 4000A) equipped with TCD detector. Figure 5 shows the H_2-TPR profiles of different

morphologies MnO_2 samples. For the NF sample, two different peaks can be observed. For NC and NT samples, the two peaks basically meet together, and the peak can also be disintegrated into two peaks. The former peak can be attributed to the reduction from MnO_2 to Mn_3O_4, and the latter is attributed to the reduction from Mn_3O_4 to MnO [1,20,21]. It is worth noting that the reduction temperature assigned to the reduction of MnO_2 to Mn_3O_4 for NF is 300°C which is lower than other samples, implying that NF sample possesses the lowest activation energy for oxygen reduction. According to previous literatures [21], the catalytic performance of a complete oxidation reaction is coincided with the low-temperature reducibility.

Figure 5. H_2-TPR of MnO_2 samples: a (NF), b (NC), c (NT), d (NS).

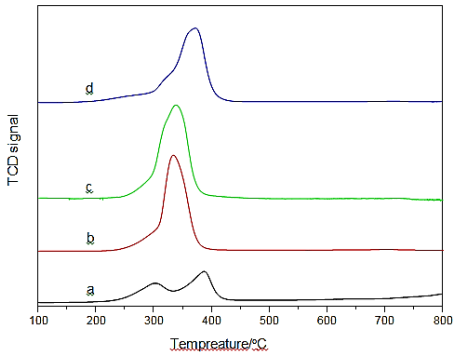

Temperature-programmed exchange reaction

The oxygen isotope exchange experiments were carried out in a U-shaped quartz reaction tube. The mass spectrometer was connected to this cycle system. In the temperature- programmed exchange experiment, $^{18}O_2$ was introduced at 200°C. After the programmed temperature rise was started, the temperature rise rate was set to 2°C/min, and the temperature rose to 650°C.

The experiments on the four samples with the temperature- programmed exchange reaction have been made. The results of the cumulative number of oxygen atoms exchanged Ne were shown in Figure 6 and the evolution of the rate of exchange Re were shown in Figure 7.

As shown in equations 3 and 4, with the increase of temperature, $^{18}O^{18}O$ (g) in the gas phase will react with ^{16}O (s) in the sample, then generate $^{16}O^{18}O$ (g). $^{16}O^{18}O$ (g) will continue to react with ^{16}O (s) to generate $^{16}O^{16}O$ (g). The mass spectrometer can monitor the reaction process and obtain the corresponding data. As can be seen from Figure 6, with the increase of temperature, the Ne of exchanged oxygen atoms will increase. In Figure 6, it can be seen that there are obvious activation differences for the four samples with the temperature increasing. The total number of oxygen atoms exchanged at 650°C is similar for NF, NC and NT. The temperature of exchange for NF sample starts from 300°C. Nevertheless, for NC and NT, the temperature is 380°C. For NF, NC and NT, two steps (low temperature and high temperature) are observed in Figure 7. The two steps can be ascribed to the surface and bulk oxygen activation [12], respectively. Because of the limited exchange for NS sample, only one step can be observed.

Figure 6. Evolution of the number of exchanged oxygen atoms (Ne) versus temperature of reaction over MnO_2.

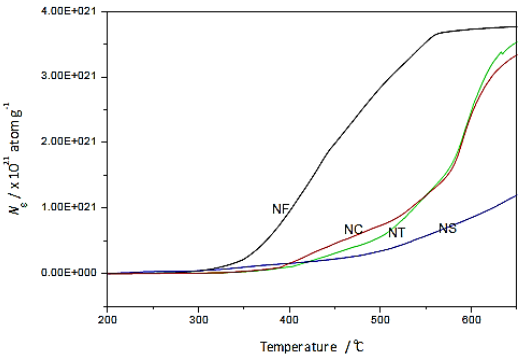

Figure 7 shows the evolution of the exchange rate (R_e) versus temperature increasing for the prepared MnO_2 samples. As shown in equations 3 and 4, with the increase of temperature, the relationship between $^{18}O^{18}O$ (g), 16O(s), $^{16}O^{18}O$ (g) and $^{16}O^{18}O$(g) has been mentioned before. The mass spectrometer can monitor the reaction process and obtain the corresponding data. The Exchange Rate (R_e) results clearly reveal that the deviation in oxygen mobility among these samples. The evolution of exchange rate versus temperature should give a maximum value (R_e^{max}) when the equilibrium of the ^{18}O concentration between the gas phase and the solid is achieved in the range of temperature recorded. The different samples can be compared considering the temperature corresponding to the R_e^{max} [12]. There is an inverse relationship between R_e^{max} and oxygen mobility (The lower R_e^{max} temperature, the higher oxygen mobility exaltation). The order obtained in terms of oxygen reactivity in the solids is of NF (440˚C)>NC (595˚C)>NT (595˚C)>NS. For NS, the temperatures corresponding to the value of R_e^{max} is higher than 600°C. Hence, within the tested temperature range, the R_e^{max} cannot be obtained. Particularly, NS sample showed the lowest exchange rate (R_e). Under normal circumstances, the low-temperature redox properties may cause the good oxygen-transfer ability. Based on the above results, it is clear that the NF sample has the best exaltation of the bulk oxygen mobility in the four samples (the lowest temperature at R_e^{max}), while the NS is the worst. After the experiment, we tested the samples by SEM. The morphology of the samples maintained good consistency with that before the test, and there was no obvious change.

Figure 7. Evolution of the exchange rate (R_e) versus temperature of reaction over MnO_2.(Note: ■: NF, ●: NC, ▲: NT, ★: NS.)

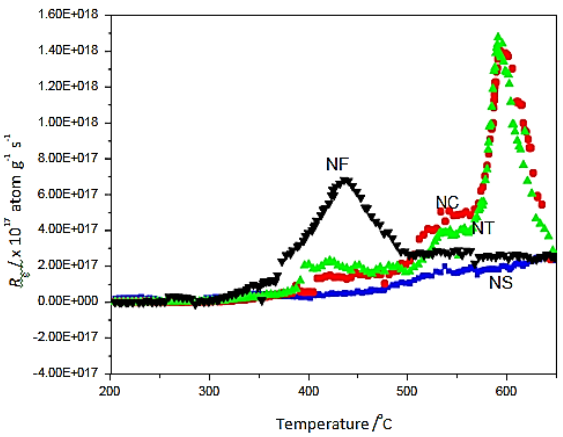

Catalytic activity test

The CO is used to determine the activity of MnO_2 samples with diverse morphologies. As seen from Figure 8, CO conversion is improved with the increasing of reaction temperature. It is verified that catalytic performance of a transition- metal oxide is associated with the surface area, oxygen ad- species, and reducibility based on the present study. The NF sample exhibits excellent catalytic activity for CO oxidation which shows the largest specific surface area and provides the most catalytic active sites in the four samples. In general, the specific surface area can greatly influence the catalytic activity. In this report, the specific surface area of the NF (97.3 m^2/g) is much larger than that of the NS (18.2 m^2/g), and the catalytic activity of the former is much better compared to that of the latter. The results indicate that the catalytic activities of the MnO_2 samples are significantly correlated with the specific surface area. According to oxygen isotopic exchange reaction, the materials which possess the enhancement of oxygen mobility can facilitate an improvement in catalytic activity. The NF sample not only presents the highest surface reactivity but also the highest bulk oxygen mobility.

According to the present results and literatures reported, the CO combustion follows surface oxidation reduction mechanism, and the oxygen which participated in reaction is mainly the surface oxygen. In our previous work [12], this conclusion has been verified. In oxygen isotopic reaction, the NF sample showed better exchange capacity for surface oxygen, and the conclusion was verified in active experiment result.

Figure 8. CO conversion versus reaction temperature for: (Note: ■: NF, ●: NC, ▲: NT, ★: NS.)

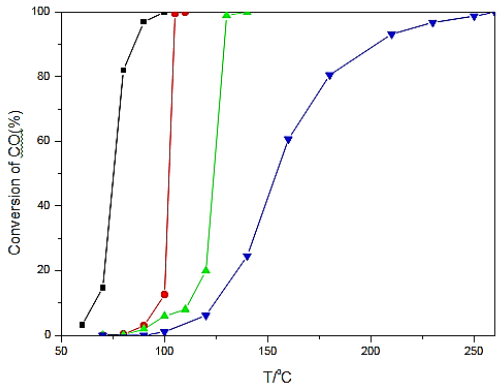

CONCLUSION

We In this work, by hydrothermal and calcinating methods, the MnO_2 samples of Nanoflower (NF), Nanococoon (NC), Nanotube (NT) and Nanoslice (NS) have been synthesized. Physicochemical properties of these materials are characterized by XRD, N_2 sorption, SEM, XPS, H2-TPR. NS sample with the highest O_{ads}/O_{latt} (1.15) mole ratio is considered to present a significant advantage in catalytic oxidizing atmosphere and the extraordinary ability of adsorption and activation of O_2 molecules, which favors CO catalytic oxidation at low- temperature region. And by Oxygen Isotopic Exchange (OIE) technology, their transfer abilities for oxygen are evaluated for the first time. The results show that NF sample (Surface area=97.3 m^2/g) possesses much higher adsorbed oxygen and much better

low-temperature reducibility than other samples. In the $^{18}O_2$ exchange reaction, the NF sample shows the best transfer ability for surface and bulk oxygen. It is concluded that the excellent catalytic performance towards CO over NF-MnO_2 sample is associated with abundant specific surface area, surface oxygen species concentration, good low temperature reducibility and better transfer ability for oxygen.

CONFLICTS OF INTEREST

There are no conflicts to declare.

ACKNOWLEDGEMENTS

The authors gratefully acknowledge the financial support from the Quanzhou science and Technology Bureau. We also thank the status of the Quanzhou Yunjian Measurement Control and Perception Technology Innovation Research Institute who gave much assistance for the paper's experiment.

REFERENCES

1. Liang S, et al. Effect of phase structure of MnO_2 nanorod catalyst on the activity for CO oxidation. J Phys Chem C. 2008;112:5307–5315.
2. Cui Y, et al. CO Oxidation over metal oxide (La_2O_3, Fe_2O_3, PrO_2, Sm_2O_3, and MnO_2) doped CuO-based catalysts supported on mesoporous $Ce0.8Zr0.2O_2$ with intensified low-temperature activity. Catalysts. 2019;9: 724.
3. Zhang Z, et al. Hydroxyl promoted preferential and total oxidation of CO over ε-MnO_2 catalyst. Catal. 2020;355;214-221.
4. Gao J, et al. Tuning chemical bonding of MnO_2 through transition-metal doping for enhanced CO oxidation. J Catal. 2016; 341:82-90.
5. Zhang J, et al. Design and preparation of MnO_2/CeO_2–MnO_2 double-shelled binary oxide hollow spheres and their application in CO oxidation. ACS Appl Mater Interfaces. 2016;8:8670-8677.
6. Liu N, et al. Preparation of a thin-film Pt electrocatalyst by MnO2 electrodeposition and galvanic replacement reaction for oxidation of methanol. J Electroanal Chem. 2019; 853:113553.
7. Yuan GH, et al. Evolution of n$C_{16}H_{34}$-water–mineral systems in thermal capsules and geological implications for deeply-buried hydrocarbon reservoirs. Geosci Front.2022;13:101322.
8. Yu XH, et al. Facile controlled synthesis of Pt/MnO_2 nanostructured catalysts and their catalytic performance for oxidative decomposition of formaldehyde. J Phys Chem C. 2012;116: 851-860.
9. Li J, et al. Effect of MnO_2 morphology on the catalytic oxidation of toluene over Ag/MnO_2 catalysts. Appl Surf Sci. 2016;385:234.
10. K. Li, et al. Synthesis of manganese dioxide with different morphologies for thallium removal from wastewater. Environ Manag Today. 2019;251:109563.
11. Zhou Z, et al. Degradation of organic pollutants by peroxymonosulfate activated by MnO2 with different crystalline structures: Catalytic performances and mechanisms. Chem Eng. 2019;374:170.
12. Yang W, et al. Activity of perovskite-type mixed oxides for the low-temperature CO oxidation: Evidence of oxygen species participation from the solid. J Catal. 2012; 295:45.
13. Cheng FY, et al. MnO_2-Based Nanostructures as Catalysts for Electrochemical Oxygen Reduction in Alkaline Media. Chem Mater. 2010; 22:898.
14. Chen WM, et al. Controllable synthesis of hollow bipyramid β-MnO_2 and Its high electrochemical performance for lithium storage. ACS Appl Mater Interfaces. 2012; 4:3047

15. Liang SH, et al. Effect of phase structure of MnO_2 nanorod catalyst on the activity for CO oxidation. J Phys Chem C. 2008;112: 5307.

16. Jiang H. Nanostructured ternary nanocomposite of rGO/CNTs/MnO_2 for high-rate supercapacitors. ACS Sustainable Chem Eng. 2014; 2:70.

17. Zhou C. MnO_2/CNT supported Pt and PtRu nanocatalysts for direct methanol fuel cells. Langmuir. 2009; 25:7711.

18. Sumanta KM, et al. Ultralayered Co_3O_4 for high-performance supercapacitor applications. J Phys Chem C. 2011;115: 15646.

19. Liu C, et al. Structure and catalytic performances of nanocrystalline Co_3O_4 catalysts for low temperature CO oxidation prepared by dry and wet synthetic routes. J Mol Catal A Chem. 2013; 370:1.

20. Ramesh K. Re-investigating the CO oxidation mechanism over unsupported MnO, Mn_2O_3 and MnO_2 catalysts. Catal. 2008;131:477.

21. Wang F, et al. Manganese oxides with rod-, wire-, tube-, and flower-like morphologies: highly effective catalysts for the removal of toluene. Environ Sci Technol. 2012; 46:4034.